

## Calculated interband optical transition spectra of GdN

Chandrima Mitra and Walter R. L. Lambrecht

*Department of Physics, Case Western Reserve University, Cleveland, Ohio 44106-7079, USA*

(Received 1 August 2008; published 7 November 2008)

The imaginary part of the dielectric function  $\text{Im}[\epsilon(\omega)]$  of rocksalt GdN is calculated using the linear muffin-tin orbital method in the atomic sphere approximation. The local spin-density approximation with added Hubbard- $U$  terms (LSDA+ $U$ ) is used to include orbital-dependent Coulomb interactions for the Gd  $4f$  and  $5d$  orbitals. The spin-orbit coupling is shown to affect the dominant spin character of the bands only negligibly so that we can analyze the optical interband transitions as being between bands of equal spin only. The separate band-to-band contributions to  $\text{Im}[\epsilon(\omega)]$  are analyzed as well as the origin of the main peaks in the Brillouin zone, allowing us to identify critical-point transitions. We find that the transitions from the upper valence band (doubly degenerate along some portions of the Brillouin zone) dominate the spectrum. The transitions to the minority-spin  $f$  bands occur as a double peak near 5.5–6 eV. The corresponding transitions of the filled  $f$  bands to the conduction band have negligible contribution. Many of the peaks correspond to complex avoided band crossings in the conduction band where local maxima and minima occur.

DOI: [10.1103/PhysRevB.78.195203](https://doi.org/10.1103/PhysRevB.78.195203)

PACS number(s): 78.20.Ci, 78.40.Fy

### I. INTRODUCTION

GdN is a bulk ferromagnetic semiconductor, which has recently attracted significant new interest both experimentally<sup>1–6</sup> and theoretically.<sup>7–12</sup> Its ferromagnetic behavior even for stoichiometric GdN was established by Li *et al.*,<sup>1</sup> its semiconducting property was definitively established by Granville *et al.*<sup>2</sup> using transport properties, and the theoretically predicted redshift of the gap<sup>13</sup> below the Curie temperatures was demonstrated experimentally by Trodahl *et al.*<sup>3</sup> Other studies by Leuenberger *et al.*<sup>5,6</sup> showed that the ferromagnetic transition is close to or coincides with a metal-insulator transition, although this may be related to defects. Several recent studies also pointed out the importance of the strain in thin films on some of these properties.<sup>4,6,7</sup> Magnetic exchange interactions were studied by Larson *et al.*<sup>7,8,10,11</sup> Band-structure calculations were presented by these same authors as well as Ghosh *et al.*<sup>9</sup> who also studied optical response functions in the interband transition regime. While optical spectra in the visible-UV range probing interband transitions have not yet been measured, except near the gap,<sup>3</sup> it is useful to further study the relation between optical response functions and the band structure in order to facilitate future experimental studies of the band structure via a determination of interband optical transitions. This is the goal of the present paper.

### II. COMPUTATIONAL APPROACH

The underlying theoretical approach used is the density-functional theory<sup>14,15</sup> within the local spin-density approximation (LSDA). For systems with narrow  $f$  bands, however, it is important to treat the orbital dependence of the Coulomb interactions. We do this using the LSDA+ $U$  formalism.<sup>16–18</sup> The  $5d$  bands in Gd are not narrow but make up the bottom of the conduction band. The LSDA approximation usually underestimates band gaps. Therefore, it is also useful to include orbital-dependent Coulomb interactions for the  $d$  electrons. This effectively allows us to shift the conduction band

up slightly so as to open a band gap adjusted to experiment. In this method the screened Coulomb and exchange energy of the  $d$  and  $f$  orbitals are first added to the LSDA functional. This is particularly important for open-shell systems in which case orbitals with certain  $m$  magnetic quantum number  $m = -\ell, \dots, \ell$ , for a given angular momentum  $\ell$ , are occupied and others are not. More precisely, the density matrix corresponding to the orbitals treated at the LSDA+ $U$  level is determined self-consistently. Then in order to avoid double counting their  $m$  orbital independent average is subtracted from it. It is important to recognize that the parameters  $U_f$  and  $U_d$  in the LSDA+ $U$  method are semiempirical. For a half-filled band as in Gd, only the effective  $U_f - J_f$  comes into play. We assume that the exchange integral  $J_f$  is unscreened and use the atomic value of 1.2 eV. The  $U_f = 9.2$  eV in our case has essentially been fixed by the experimentally known splitting between occupied and empty  $f$  orbitals in the series of Gd-pnictides.<sup>19</sup> It was shown to also lead to the correct occupied  $f$  band position in GdN.<sup>10</sup> The  $U_d$  is adjusted to give the correct band spin-averaged direct gap at  $X$  as determined by Trodahl *et al.*<sup>3</sup> Our band structures obtained with this approach are in good agreement with a recent  $GW$  ( $G$  for the Green's function and  $W$  for screened Coulomb interaction) calculation by Chantis *et al.*,<sup>12</sup> except for the position of the empty  $f$  bands. The latter has a marked discrepancy from experiment in that  $GW$  calculation, as discussed in their paper. While Ghosh *et al.*<sup>9</sup> also used the LSDA+ $U_d+U_f$  approach, they still obtain a semimetallic band structure. The difference is in the choice of parameters. As mentioned, ours are chosen to incorporate the most recent experimental findings on the material.

In contrast to previous band-structure investigations from our research group<sup>10,11</sup> which used a full-potential-linearized muffin-tin orbital method (FP-LMTO),<sup>20</sup> we use here the atomic sphere approximation (ASA).<sup>21–24</sup> While in principle, optical matrix elements can also be calculated in FP-LMTO, this has not yet been implemented in the code presently available to us, while it has been in the ASA version of LMTO. The latter should be quite accurate for a structure with high symmetry as is the rocksalt structure and, in any

case, we can check the accuracy of our band structures against the FP-LMTO results and make adjustments, for example, by using different sphere radii where needed. ASA is more sensitive to sphere radii because it does not include explicitly an interstitial region representation of the wave functions but instead uses slightly overlapping space-filling spheres and makes implicit assumptions about the behavior of the wave function outside these spheres. We find that this is even more crucial for the LSDA+U approach with  $f$  electrons as will be discussed in more detail below. Also, the  $U_f$  value need not be the same as in FP-LMTO because it is essentially applied as a projection operator  $\pm \frac{U_f - J_f}{2} |\phi_f\rangle\langle\phi_f|$ , where plus and minus signs refer to unoccupied and occupied spin states, respectively. As such, it depends on the actual orbitals  $\phi_f$  inside the spheres which depend somewhat on sphere radius. The  $6s$ ,  $5p$ ,  $5d$ , and the  $4f$  Gd orbitals are taken as valence states. Although the completely filled  $5p$  bands are rather deep and semicorelike, they still have a significant dispersion and are thus preferably treated as band rather than core states. To sample the Brillouin zone in the self-consistent calculations, a shifted Monkhorst-Pack<sup>25</sup>  $6 \times 6 \times 6$  mesh was used and was found to be sufficiently converged. We perform our calculations at the experimental lattice constant. The present LSDA+U method has been shown to also reproduce well the structural and total-energy properties.<sup>10,11</sup>

The imaginary part of the dielectric function is calculated in the long-wavelength limit. The analysis of the spectrum in terms of its individual band-to-band contributions is done using

$$\text{Im}[\epsilon^j(\omega)] = \left(\frac{2\pi e}{m\omega}\right)^2 \sum_v \sum_c \int d\mathbf{k} |\langle v\mathbf{k} | p^j | c\mathbf{k} \rangle|^2 \times \delta[E_c(\mathbf{k}) - E_v(\mathbf{k}) - \hbar\omega] \quad (1)$$

with  $p^j = -i\hbar\nabla_j$  as the momentum operator, using Gaussian units. Local-field and excitonic effects are neglected in this approach. It has been found in numerous previous studies that when going beyond the present random-phase approximation (RPA) long-wave (LW) length limit, it is important to include both electron-hole coupling and local-field effects simultaneously. A few groups have implemented the Bethe-Salpeter equation approach to include such effects.<sup>26-31</sup> They provide information on how the RPA-LW dielectric function differs from the one including local-field and electron-hole interaction effects but the analysis of the optical function in terms of specific interband transitions is less obvious and transparent in those approaches. So, ultimately, one still needs to evaluate the optical response function as calculated here in order to analyze it in terms of interband transitions. Our present work thus presents only a first but important step to a more complete understanding of the optical response functions in these materials. To analyze this function the separate Brillouin-zone integrals for each band pair  $\{v, c\}$  are calculated. For the optical calculations, we used a finer  $15 \times 15 \times 15$  unshifted  $\mathbf{k}$ -point mesh and the tetrahedron integration method. One of the main effects of the electron-hole interaction is that it draws oscillator strength to Van Hove singularities in the joint density of states (JDOS). While the

present calculation tends to have peaks where the bands are approximately parallel over a rather large region of  $\mathbf{k}$  space, the electron-hole interaction increases the oscillator strength at the points where the bands are exactly parallel, in particular, near  $M_2$ -type Van Hove singularities, i.e., saddle points with minima in two directions and a maximum in one direction or near two-dimensional (2D)-like saddle points. For examples, of how these discrepancies between the RPA-LW limit, as calculated here, and the dielectric function including electron-hole interaction and hence the experiment can be analyzed once good experiments are available, we refer the reader to prior studies of GaN (Ref. 32) and CdSe.<sup>33</sup> Unfortunately, at present no experiments of this type are available for GdN.

### III. RESULTS

#### A. Band structures

Since the optical matrix elements as written above do not affect the spin, we find transitions only between bands of the same spin character. However, spin-orbit coupling mixes the spin character of the bands. In that case, we need to be more careful with calculating the matrix elements. The requirement is that the total angular momentum (orbital and spin) of initial and final states should be connected by a nonzero matrix element of the momentum operator. Inside each sphere the wave function is expanded in partial waves and thus labeled by  $l, m, \sigma$ , with  $l, m$  labeling the orbital angular-momentum character and  $\sigma = \pm 1/2$  the spin's  $z$  component. Using spherical components of the momentum operator  $\nabla_\mu$  with  $\mu = 0, \pm 1$ , the matrix elements to be considered are  $\langle \phi_{l,m,\sigma}^u | \nabla_\mu | \phi_{l',m',\sigma'}^u \rangle$ , where  $u = 1, 2$  is used to distinguish  $\phi$  and  $\dot{\phi}$ , i.e., the partial waves at the linearization energy  $\epsilon_v$  and its energy derivative, respectively. The requirement is then that  $m + \sigma + \mu - m' - \sigma' = 0$ . If bands have a pure spin character, we will only encounter  $\sigma = \sigma'$  and hence only matrix elements obeying  $m + \mu - m' = 0$  are required; but if they are mixed, we may need additional matrix elements. We avoid this complication by performing the optical calculations without spin-orbit coupling. To justify this picture of considering transitions, only between bands of the same spin, we first check that the spin character is mostly preserved even when spin-orbit coupling is included.

As can be seen from Fig. 1 the spin character is largely preserved in the band structure even when the spin-orbit coupling is switched on. In this figure the bands are color coded with a continuous mix of colors between red and blue according to the mixing of spin up and spin down in the wave function. Thus red is pure majority spin, blue is pure minority spin, and any shade of purple in between corresponds to the degree of mixing. Unfortunately, this information is hard to convey without color and is only available in the online version

We can also see that the band structures shown here are in good agreement with the full-potential band structures of Ref. 11. We note, however, that this depends crucially on the value used of  $U_f$  and the sphere radii adopted. Here we used a value  $U_f = 9.2$  and  $s/w$  values of 1.159, 1.159, and 0.762

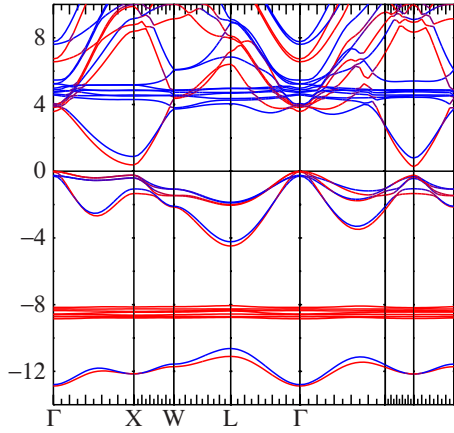


FIG. 1. (Color online) The band structure of GdN with spin-orbit coupling. Red indicates the majority-spin character while blue indicates the minority-spin character.

for Gd, N, and empty spheres, respectively, with  $w$  as the average Wigner-Seitz sphere radius and  $s$  as the ASA-sphere radius of each species. We found that if we choose Gd sphere ratios to N sphere ratios in the ratio of their atomic radii, the valence bands showed an incorrect reversed spin splitting (i.e., majority spin below minority spin). We know this is incorrect because the redshift of the gap which follows from it has been clearly established experimentally.<sup>3</sup> This indicates a lack of hybridization of the N- $p$  orbitals with the Gd- $f$ . In ASA LMTO these types of hopping matrix elements are described by  $\sqrt{\Delta_i}S_{ij}\sqrt{\Delta_j}$  with  $S_{ij}$  as the structure constant and potential parameters  $\sqrt{\Delta_{Rl}}=-\sqrt{2/w}W\{J_{Rl}^\gamma, \phi_{Rl}\}$  with  $i$  and  $j$  indices representing atomic site and angular momentum  $R, l, m$ . Here  $W\{f, g\}=s^2[f(s)g'(s)-f'(s)g(s)]$  is the Wronskian, the prime indicating the radial derivative, and  $J^\gamma$  is the mix of spherical Bessel and Neumann functions that matches onto the  $\phi^\gamma$  function which is orthogonal to the  $\phi$  function in the sphere, also known as the nearly orthogonal representa-

tion. The point is that this potential parameter goes to zero if the wave function  $\phi$  and its radial derivative are both going to zero at the sphere boundary. Thus for a very localized orbital as the Gd  $f$  and a large sphere, it becomes numerically too small to describe the coupling between Gd  $f$  and N- $p$  correctly. While in FP-LMTO the matrix elements are calculated correctly regardless of the choice of spheres because the interstitial region is included explicitly, more care is needed for the ASA. We are thus forced to choose the Gd and N spheres more or less of equal radius. We still do not want to make them too small by keeping a relatively smaller empty sphere compared to the actual atom spheres. While some dependence on this choice of parameters is unavoidable, the band structure thus obtained is in satisfactory agreement with the full-potential one.

Finally, for reference in Sec. III B, we present the bands of major interest to the optical transitions of majority and minority spin separately, including symmetry labels in Fig. 2. The main difference between the two is the presence of the seven flat empty Gd- $f$  bands. These bands are only labeled at the  $\Gamma$  point. The symmetry labeling uses the standard notations of Bouckaert *et al.*<sup>34</sup>

**B. Analysis of the optical response**

The  $\text{Im}[\epsilon(\omega)]$  and  $\text{Re}[\epsilon(\omega)]$  for the minority and majority spins are shown in Fig. 3. The part of the spectrum between 8 and 10 eV shows a strong similarity for both spins. The part below 5 eV is clearly coming only from the near gap part and shows considerable difference indicative of the strong spin polarization of the top valence and bottom conduction bands. The main extra peak in minority-spin spectrum at about 5–7 eV can already be assigned to transitions from the valence band to the minority  $f$  bands since these bands are absent from majority spin. The counterpart transitions from occupied  $f$  to conduction bands are much weaker and would occur only above 12 eV where they are swamped

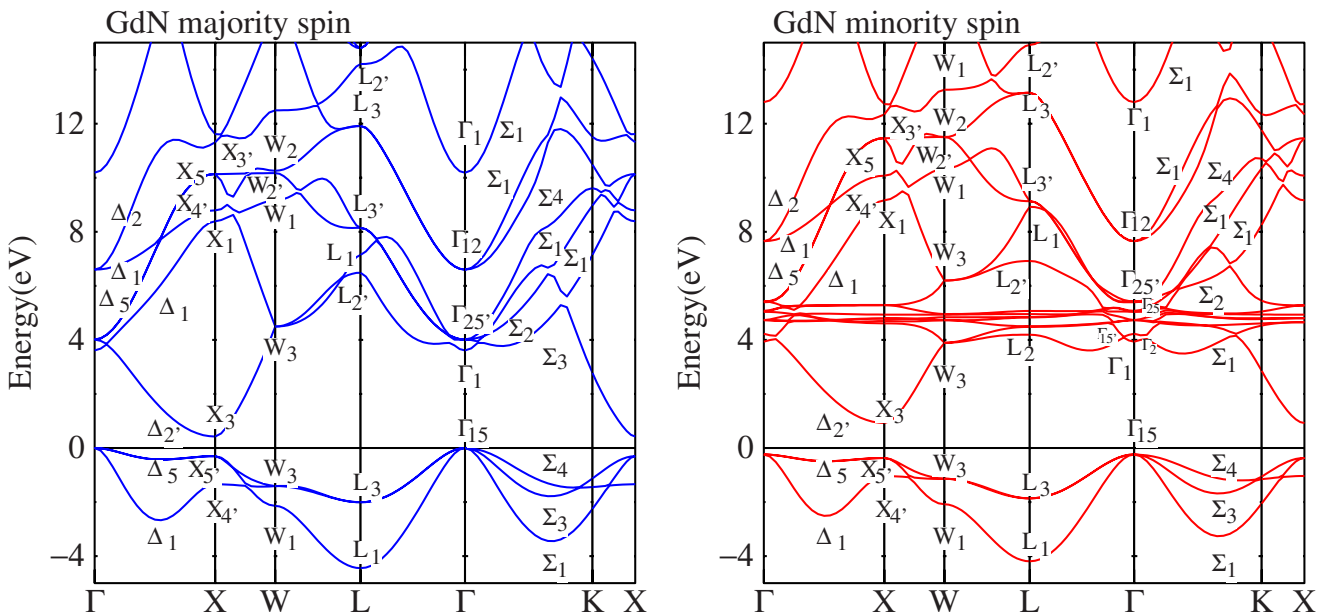


FIG. 2. (Color online) Majority- (left) and minority- (right) spin bands of GdN with symmetry labeling.

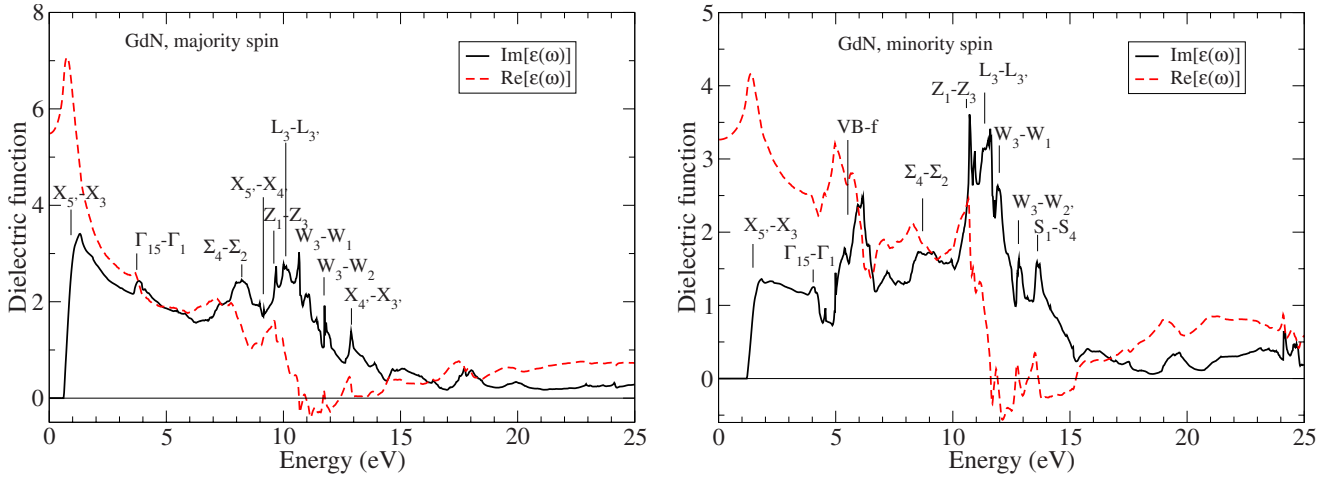


FIG. 3. (Color online) Real (dashed red) and imaginary (black solid) parts of the dielectric function of GdN for majority (left graph) and minority spins (right graph). Critical points associated with the peaks are indicated.

by the transitions between valence band and higher conduction bands. We have indicated some critical-point transitions whose correspondence to the peaks is discussed below.

We note that these spectra show considerable more structure than shown for  $\text{Im}[\epsilon(\omega)]$  by Ghosh *et al.*<sup>9</sup> However, that author shows also the optical conductivity, which is proportional to  $\omega \text{Im}[\epsilon(\omega)]$  in the range 0–10 eV. For a comparison we show also the optical conductivity spectrum in Fig. 4.

Although, we will primarily analyze the  $\text{Im}[\epsilon(\omega)]$  function because it is most directly related to the interband transitions, its measurement requires either Kramers-Kronig transformation from the reflectivity measurements or spectroscopic ellipsometry. Since the reflectivity is one of the more directly measurable quantities, we show it in Fig. 5. We show here both the individual spin contributions and their sum, which is the only directly measurable quantity. Comparing the reflectivity with the dielectric function curves, we see that the reflectivity stays high at higher energies than  $\text{Im}[\epsilon(\omega)]$  and its high-energy peaks do not correspond directly to interband transitions but to the structure in the

$\text{Re}[\epsilon(\omega)]$ . We note that our reflectivity looks significantly different from that given by Ghosh *et al.*<sup>9</sup> This is primarily because we have a semiconducting band structure, whereas he has a semimetallic band structure and hence his spectrum is dominated by the intraband transitions at low energy.

Generally speaking in all of these spectra, we can see similar features for both spin with the minority-spin features slightly higher in energy than the corresponding majority-spin feature as expected. The only deviation from this rule is that only in the minority-spin case, we see transitions to the extra empty *f* bands.

We now separately analyze the optical response function for majority and minority spins. We start with majority spin because it is slightly simpler; no transitions involving the *f* bands are involved. In Fig. 6 we show on the left the interband differences between the top valence band and several of the conduction bands plotted along symmetry lines of the Brillouin zone. On the right, we show the corresponding contributions to the  $\text{Im}[\epsilon(\omega)]$  along with the total. First of all, this shows which band pair contributes mostly to each peak. Second, we can now make a correspondence between the

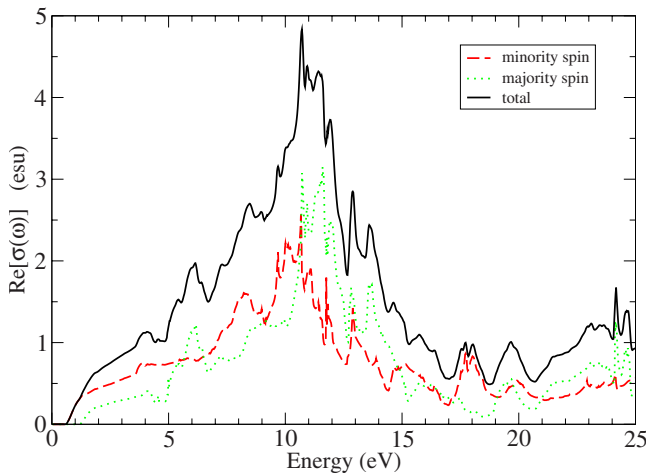


FIG. 4. (Color online) Optical conductivity  $\text{Re}[\sigma(\omega)]$  (solid black line) and its separate spin components; minority spin (red dashed) and majority spin (green dotted).

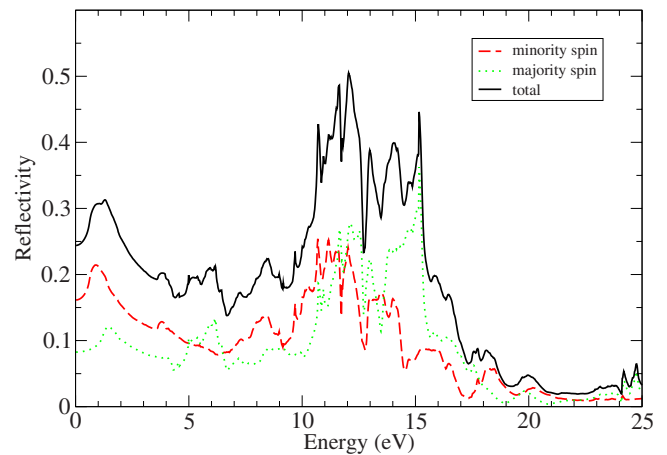


FIG. 5. (Color online) Total reflectivity (solid black line) decomposed in its minority (dashed red) and majority (dotted blue) components.

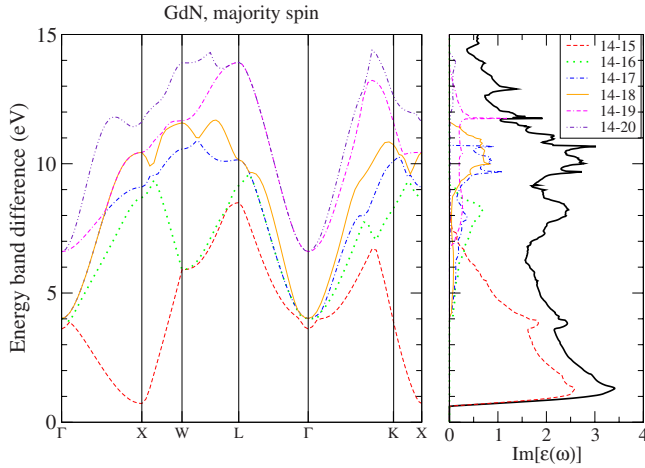


FIG. 6. (Color online) Energy-band differences between conduction bands and highest valence band (No. 14) for majority spin in GdN on the left and the corresponding contributions to the  $\text{Im}[\epsilon(\omega)]$  shown in thick solid (black) line for the total and corresponding line types and colors for the individual contributions.

major peaks in each contribution to regions of the Brillouin zone where the corresponding band difference is flat, meaning that the bands are parallel and hence the largest joint density of states occurs. Often, these correspond to Van Hove singularities called critical points. Although not included here, the electron-hole interaction tends to further enhance the peaks at these points because the electron and hole have exactly the same velocity, which enhances their interactions and leads to an enhanced spectral weight in the optical function.

We start with the transition between the upper valence band and the lowest conduction band. For majority spin in our counting, which starts from the  $5p$  valence bands, these are bands 14 and 15. In fact, there are three Gd- $5p$  bands, one N  $2s$ , seven Gd- $4f$ , and three N- $2p$  valence bands of majority spin. The onset occurs obviously at the  $X$  point and only the region of the Brillouin zone near the  $\Delta=\Gamma$ - $X$  line can contribute at low energy. The band difference is very steep along the  $X$ - $W$ - $Z$  and  $X$ - $K$ - $S$  lines, so only a small tube along the  $\Delta$  line contributes in this energy range. Hence the JDOS is quasi-one-dimensional and this explains the sharp onset which almost looks like a  $1/\sqrt{E}$ -type Van Hove singularity.

Next, let us consider the selection rules along the  $\Delta$  line. The point group for this line is  $C_{4v}$ . A vector along  $z$  has the  $\Delta_1$  symmetry for the  $\Delta$  line along  $[001]$  and hence allows transitions between any two bands of the same symmetry for light electric-field polarization along  $z$ . A vector along  $x$  or  $y$  has  $\Delta_5$  symmetry. Because  $\Delta_5 \otimes \Delta_5 = \Delta_1 \oplus \Delta_2 \oplus \Delta_2' \oplus \Delta_1$ , transitions from a  $\Delta_5$  band (the upper valence band) to any other symmetry band are allowed for light polarization perpendicular to the  $\Delta$  line in question. Also,  $\Delta_5 \otimes \Delta_i = \Delta_5$  for  $i = 1, 1', 2, 2'$ . In short, all transitions from  $\Delta_5$  are allowed. In particular, the transition we consider here is the  $\Delta_5$ - $\Delta_2'$  transition and is allowed for light polarization perpendicular to this line. These are N- $2p$  to Gd- $d_{xy}$  transitions. Of course, the only nonzero matrix elements occur inside each sphere, but both these bands have some hybridization between Gd and

N. In other words, the tails of the Gd  $d$  stick into the N spheres and vice versa; the tails of the N- $p$  orbitals stick into the Gd spheres. Still, we can think of this as a charge-transfer transition between the two atoms. Near the  $\Gamma$  point, the lowest band has  $\Delta_1$  symmetry. This is the bottom of the mainly Gd- $6s$ -like band. This transition is also allowed and gives a second onset. We can see that the small peak at 3.9 eV corresponds to the transitions at the  $\Gamma$  point between the  $\Gamma_{15}$  valence-band maximum and the  $\Gamma_1$  conduction band. These are allowed by the selection rules because a vector has  $\Gamma_{15}$  symmetry and  $\Gamma_{15} \otimes \Gamma_1 = \Gamma_{15}$ .

Next, we consider transitions from the upper valence to the second conduction bands. This gives a somewhat rounded peak centered at about 8 eV. We can see that the onset of this peak falls near the wiggle in the band difference along the  $\Sigma$  direction. We thus can label this peak as a  $\Sigma_4$ - $\Sigma_2$  transition. The peak falls pretty much at the energy of the  $K$  point even though this is not strictly a high-symmetry point and does not correspond to a Van Hove singularity. On the other hand, there is a Van Hove singularity at the  $X$  point in this band difference. Near  $X$  this band difference goes down toward  $\Gamma$ , but it goes up in the perpendicular directions in the square face of the fcc Brillouin zone: this is an  $M_1$ -type Van Hove singularity where the corresponding JDOS should diverge in slope coming from below. One can barely see this because there is no extended region of  $k$  space with flat bands associated with it. Nevertheless, this point, which is the  $X_5$ - $X_1$  critical point might become enhanced by electron-hole interactions and is expected at about 8.7 eV.

In the transitions from the upper valence to the third conduction bands, we see three sharp peaks. The first peak at 9.6 eV corresponds to the little flat region along  $X$ - $W$ - $Z$ , the middle peak at 10.1 eV occurs near the  $L$ -point energy for  $L_3$ - $L_{3'}$ , and the highest peak at 10.7 eV lies just above the  $W$  point, so we can label it as  $W_3$ - $W_1$ . The symmetries along  $Z$  for these bands are  $Z_1$  and  $Z_3$ , respectively, so we can label the first peak a  $Z_1$ - $Z_3$  transition. Roughly we can say that these three peaks are associated with relatively parallel bands along the whole Brillouin-zone surface. There is also a lower peak at about 7.9 eV which again is associated with the complex band crossings along  $\Sigma$ . Along  $\Sigma$  (point group  $C_{2v}$ ) only the transitions between  $\Sigma_1$  and  $\Sigma_2$  are forbidden but the valence-band maximum has symmetry  $\Sigma_4$  so all transitions from it are allowed. The  $X_5$ - $X_4$  critical point is also associated with this band pair and may be expected to be enhanced by electron-hole interaction effects. Its energy occurs just below the first peak in this region. It is an  $M_1$ -type singularity. The  $L_3$ - $L_{3'}$  critical-point transition looks more like a 2D saddle point because the band difference is relatively flat in the hexagonal face of the Brillouin zone near  $L$  but at a maximum along the  $\Gamma$ - $L$  line. We note that also along  $\Lambda=\Gamma$ - $L$  all transitions are allowed. The point group here is  $C_{3v}$ . A vector along the  $\Lambda$  line belongs to  $\Lambda_1$ ; a vector perpendicular to the line belongs to  $\Lambda_3$  representations. The former allows transitions between bands of the same symmetry and the latter allows transitions between all symmetries because  $\Lambda_3 \otimes \Lambda_3 = \Lambda_1 \oplus \Lambda_2 \oplus \Lambda_3$  and  $\Lambda_3 \otimes \Lambda_i = \Lambda_3$  for  $i = 1, 2$ .

Transitions from bands 14 to 18, the fourth valence band, give a peak mostly in the same energy region as 14-17. The sharp features on it are associated with several wiggles in the

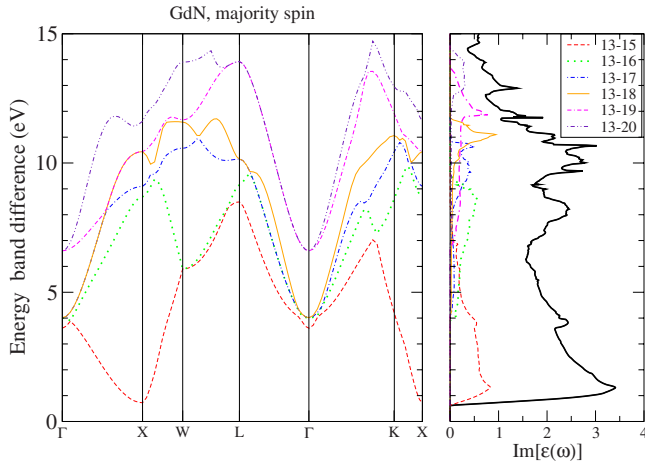


FIG. 7. (Color online) Energy-band differences between conduction bands and second highest valence band (No. 13) for majority spin in GdN on the left and the corresponding contributions to the  $\text{Im}[\epsilon(\omega)]$  shown in thick solid (black) line for the total and corresponding line types and colors for the individual contributions.

band difference along  $X$ - $W$ = $Z$ ,  $W$ - $L$ = $Q$ , and along  $\Lambda$  near  $L$ . The latter coincides precisely with the peak at 9.6 eV we encountered earlier and inspection of the bands shows that this occurs because of the band crossing along  $\Lambda$  and the peak corresponds to the maximum of the  $\Lambda_1$  band which joins the  $\Gamma_{25'}$  with the  $L_1$  point. Finally, in the transitions to band 19, we see a very sharp peak at 11.8 eV, which clearly comes from the very flat band difference near  $W$  and which we thus label as  $W_3$ - $W_{2'}$ . Note that the  $W_2$  and  $W_{2'}$  are very close to each other.

The contributions from transitions between band 13 and the conduction bands are shown in Fig. 7. We can see a great similarity with the transitions from band 14. This is no surprise because the top two valence bands are degenerate along  $\Delta$  and  $\Lambda$  and nearly degenerate along  $X$ - $W$ . The structure of the peaks mostly reflects the conduction-band structure as was already seen in the previous discussion and thus some of the peaks associated with structure along  $\Sigma$  are just slightly displaced to higher energy because this band is slightly lower along that direction. Again all transitions are allowed.

The transitions originating in band 12 are shown in Fig. 8. First, we see that most of these make only a small contribution to the overall dielectric function. Note that we have multiplied them by a factor of 5 to make them visible. Along  $\Delta$  this band has  $\Delta_1$  symmetry. Only transitions to bands of symmetry  $\Delta_1$  are allowed for polarization along this axis and to bands of symmetry  $\Delta_5$  for polarization perpendicular to the axis. Thus, for example, transitions to the lowest conduction band of  $\Delta_2$  symmetry near  $X$  are not allowed, and even though there would have been a fairly large JDOS because the bands are rather parallel over some region, we see that the actual contribution to the optical function is small. It should be recalled that only along the symmetry line the transition is zero. At neighboring points it is not zero but small. We can again see various correlations between extrema in the band difference and the peak positions but since they are all quite weak and do not give major contributions to the peaks, we will not discuss it in detail. We only note

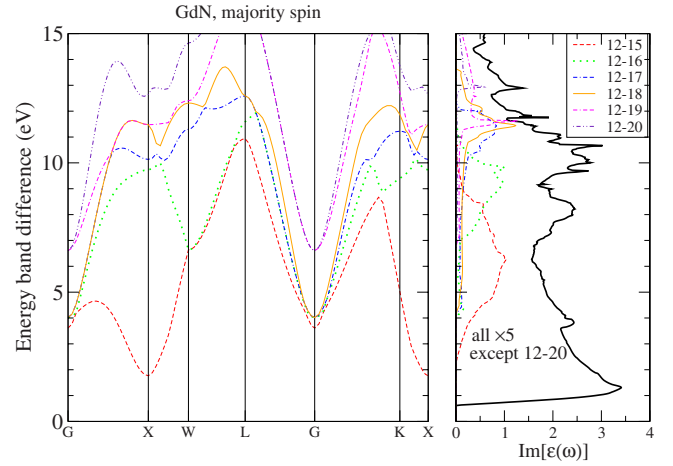


FIG. 8. (Color online) Energy-band differences between conduction bands and second highest valence band (No. 12) for majority spin in GdN on the left and the corresponding contributions to the  $\text{Im}[\epsilon(\omega)]$  shown in thick solid (black) line for the total and corresponding line types and colors for the individual contributions.

that the contribution 12-20 is sizable and gives rise to the peak at 13.0 eV, which corresponds to the singularity near  $X$  along  $X$ - $K$ = $S$  and  $X$ - $\Gamma$ . It is thus related to the  $X_{4'}$ - $X_{3'}$  critical point.

Now we turn to the minority spin. In this case, the three valence bands of interest are 5-7. The conduction-band 8 is Gd- $d_{xy}$  like near  $X$  and Gd- $s$  like near  $\Gamma$ , bands 9-15 are primarily  $f$  like, and 16-20 are Gd- $d$ -like or  $s$  like. One complication is that the  $\Lambda_1$  band starting at  $\Gamma_1$  as band 8 crosses through the  $f$  bands and becomes band 15 while band 8 is  $f$  like along this line. It connects the  $\Gamma_2$  to the  $L_2$ . Roughly speaking we expect transitions between bands  $\{6,7\}$  and  $\{8,16-20\}$  to resemble those originating in bands 13 and 14 for majority spin. There will, however, now be additional transitions to the empty  $f$  bands 9-15. We have lumped the contributions from bands 9-15 together in the dielectric function. Since the  $f$  bands are flat and the top valence band is relatively flat except between  $\Gamma$ - $L$  and  $L$ - $W$ , i.e., on the hexagonal Brillouin-zone face, we expect a large JDOS for these transitions.

The transitions originating in band 7 are shown in Fig. 9. The discussion is pretty similar to that for the majority spin. We again see an abrupt onset near the  $X_{5'}$ - $X_3$  followed by a second peak for the  $\Gamma_{15}$ - $\Gamma_1$  transition. We then see the empty  $f$  bands (bands 9-15) all collectively indicated in red dashed line giving a strong contribution to the dielectric function for the double-peaked structure at 5.5 and 6.0 eV. We can see that these two peaks correspond roughly to the minimum near  $\Gamma$  and a maximum near  $L$  and are basically flat along  $\Delta$ . Since the  $f$  bands are flat, what we see is just the upper valence-band dispersion reversed because we subtract it. Band 15 obviously disperses away because it has become the  $s$ -like conduction band and this gives this contribution its slowly decreasing high-energy tail. In the 7-16 contribution we see again a peak associated with the structure along  $\Sigma$ . In the 7-17 contribution we see peaks coming from the near band crossings along  $X$ - $K$ = $S$ : the flat region near  $L$  and the

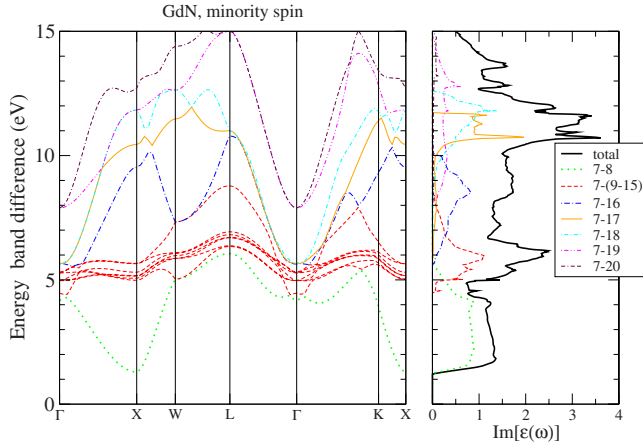


FIG. 9. (Color online) Minority-spin interband transitions starting in the highest valence band (No. 7) (left) and their contribution to  $\text{Im}[\epsilon(\omega)]$  (right).

extrema near  $W$ . All of this is very similar to what we had for the majority-spin bands but slightly shifted to higher energy because of the spin splitting of the bands.

Transitions from band 6 are similar to those from band 7 and are shown in Fig. 10. The transitions from band 5 shown in Fig. 11 are weaker as was the case also for majority spin. The sharp peak at 13.8 eV can be seen to be related to a singularity along the  $K$ - $X$ = $S$  line. The symmetry along  $S$  is the same as along  $\Sigma$ . Inspection of the band symmetries shows that we can label it as an  $S_1$ - $S_4$  transition. This peak also has some contribution from transitions between bands 7 and 20 occurring along the  $Z$  line.

From the above discussion of the peaks in  $\text{Im}[\epsilon(\omega)]$ , we have seen that most peaks correspond to some kind of extremum in the band differences and are strongly influenced by JDOS. Selection rules played only a minor role because only a few transitions (mostly from the third valence band down from the top) are forbidden. We have also seen that the strongest peaks arise from transitions from the top valence band. Several of the strong peaks were related to near band crossing related features in the conduction bands where the bands

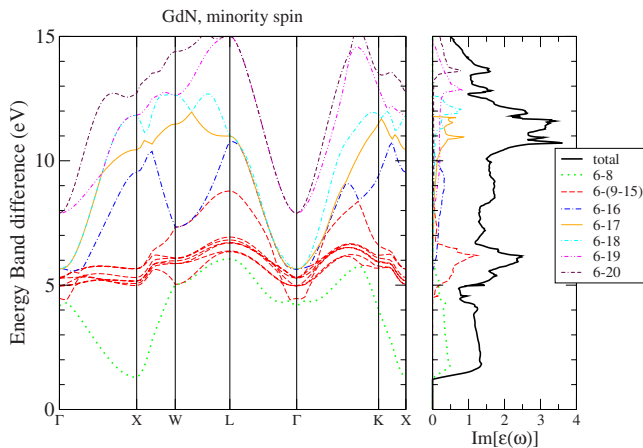


FIG. 10. (Color online) Minority-spin interband transitions starting in the second highest valence band (No. 6) (left) and their contribution to  $\text{Im}[\epsilon(\omega)]$  (right).

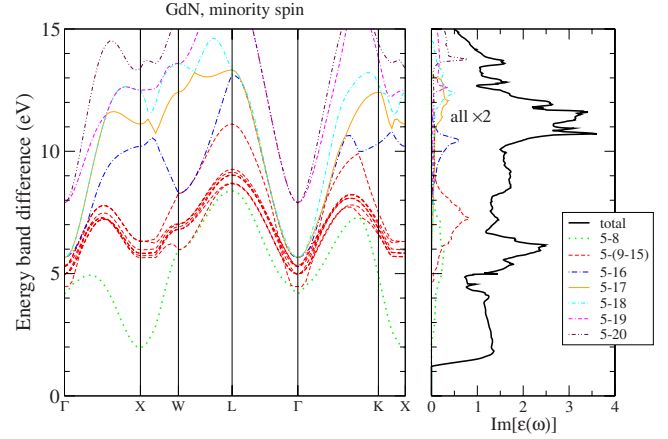


FIG. 11. (Color online) Minority-spin interband transitions starting in the third highest valence band (No. 5) (left) and their contribution to  $\text{Im}[\epsilon(\omega)]$  (right).

of the same symmetry have avoided crossings and lead to local maxima and minima. Ultimately, one is interested in using this information to obtain band differences at high-symmetry points. Their relation to the peaks can be obtained from the above figures and discussion. We give a summary of the allowed high-symmetry point transitions in Table I and have indicated their association with peaks in  $\text{Im}[\epsilon(\omega)]$  in Fig. 3. Finally, we caution that electron-hole interactions or continuum excitonic effects may still significantly shift oscillator strength in particular near  $M_1$ -type Van Hove singularities.

TABLE I. Critical-point transitions in electron volt.

Transition	Majority spin	Minority spin
$\Gamma_{15}-\Gamma_1$	3.61	4.17
$X_{5'}-X_3$	0.72	1.29
$X_{5'}-X_1$	8.69	9.53
$X_{5'}-X_{4'}$	9.09	10.44
$X_{5'}-X_5$	10.44	11.83
$X_{4'}-X_1$	9.73	10.20
$X_{4'}-X_{4'}$	10.13	11.11
$X_{4'}-X_3$	12.65	13.38
$W_3-W_3$	5.90	5.03
$W_3-W_1$	10.57	11.47
$W_3-W_{2'}$	11.58	12.63
$W_3-W_2$	11.66	12.65
$W_1-W_3$	6.63	5.98
$W_1-W_1$	11.30	12.42
$L_3-L_{2'}$	8.49	8.78
$L_3-L_1$	9.15	10.79
$L_3-L_{3'}$	10.15	11.00
$L_3-L_3$	13.92	15.01
$L_1-L_{2'}$	10.93	11.11
$L_1-L_2'$	11.59	13.12

#### IV. CONCLUSIONS

Optical spectra related to interband transitions in GdN were calculated. We showed first of all that it is useful and valid to separate these in majority and minority spin separate contributions by showing that the bands largely maintain their pure spin character even when spin-orbit coupling is included. The small spin-orbit-induced splittings can then be ignored and the spectra calculated separately for each spin. We presented real and imaginary parts of the dielectric function, the real part of the optical conductivity, and reflectivity spectra for easy future comparison to experimental data.

We presented a detailed analysis of the imaginary part of the dielectric function for each spin in separate band-to-band components and analyze them in terms of specific critical points in the Brillouin zone.

Of major importance is that we identify a peak which can clearly be assigned to transitions from the valence band to mainly the empty  $f$  bands which could thus be used experimentally to locate the energy position of these bands relative to the Fermi level. The corresponding transitions from filled  $f$  bands to conduction band, however, are weak and overwhelmed by stronger  $N 2p$  valence band to Gd  $5d$ -like conduction bands.

#### ACKNOWLEDGMENTS

This work was supported by the National Science Foundation World Materials Network program under Grant No. DMR-0710485.

- 
- <sup>1</sup>D. X. Li, Y. Haga, H. Shida, T. Suzuki, Y. S. Kwon, and G. Kido, *J. Phys.: Condens. Matter* **9**, 10777 (1997).
- <sup>2</sup>S. Granville *et al.*, *Phys. Rev. B* **73**, 235335 (2006).
- <sup>3</sup>H. J. Trodahl, A. R. H. Preston, J. Zhong, B. J. Ruck, N. M. Strickland, C. Mitra, and W. R. L. Lambrecht, *Phys. Rev. B* **76**, 085211 (2007).
- <sup>4</sup>K. Khazen, H. J. von Bardeleben, J. L. Cantin, A. Bittar, S. Granville, H. J. Trodahl, and B. J. Ruck, *Phys. Rev. B* **74**, 245330 (2006).
- <sup>5</sup>F. Leuenberger, A. Parge, W. Felsch, K. Fauth, and M. Hessler, *Phys. Rev. B* **72**, 014427 (2005).
- <sup>6</sup>F. Leuenberger, A. Parge, W. Felsch, F. Baudalet, C. Giorgetti, E. Dartyge, and F. Wilhelm, *Phys. Rev. B* **73**, 214430 (2006).
- <sup>7</sup>C.-G. Duan, R. F. Sabiryanov, J. Liu, W. N. Mei, P. A. Dowben, and J. R. Hardy, *Phys. Rev. Lett.* **94**, 237201 (2005).
- <sup>8</sup>C.-G. Duan, R. F. Sabiryanov, W. N. Mei, P. A. Dowben, S. S. Jaswal, and E. Y. Tsymlal, *Appl. Phys. Lett.* **88**, 182505 (2006).
- <sup>9</sup>D. B. Ghosh, M. De, and S. K. De, *Phys. Rev. B* **72**, 045140 (2005).
- <sup>10</sup>P. Larson and W. R. L. Lambrecht, *Phys. Rev. B* **74**, 085108 (2006).
- <sup>11</sup>P. Larson, W. R. L. Lambrecht, A. Chantis, and M. van Schilf-gaarde, *Phys. Rev. B* **75**, 045114 (2007).
- <sup>12</sup>A. N. Chantis, M. van Schilf-gaarde, and T. Kotani, *Phys. Rev. B* **76**, 165126 (2007).
- <sup>13</sup>W. R. L. Lambrecht, *Phys. Rev. B* **62**, 13538 (2000).
- <sup>14</sup>P. Hohenberg and W. Kohn, *Phys. Rev.* **136**, B864 (1964).
- <sup>15</sup>W. Kohn and L. J. Sham, *Phys. Rev.* **140**, A1133 (1965).
- <sup>16</sup>V. I. Anisimov, J. Zaanen, and O. K. Andersen, *Phys. Rev. B* **44**, 943 (1991).
- <sup>17</sup>V. I. Anisimov and O. Gunnarsson, *Phys. Rev. B* **43**, 7570 (1991).
- <sup>18</sup>A. I. Liechtenstein, V. I. Anisimov, and J. Zaanen, *Phys. Rev. B* **52**, R5467 (1995).
- <sup>19</sup>H. Yamada, T. Fukawa, T. Muro, Y. Tanaka, S. Imada, S. Suga, D.-X. Li, and T. Suzuki, *J. Phys. Soc. Jpn.* **65**, 1000 (1996).
- <sup>20</sup>M. Methfessel, M. van Schilf-gaarde, and R. A. Casali, in *Electronic Structure and Physical Properties of Solids: The Use of the LMTO Method*, Lecture Notes in Physics Vol. 535, edited by H. Dreyssé (Springer-Verlag, Berlin, 2000), p. 114.
- <sup>21</sup>O. K. Andersen, *Phys. Rev. B* **12**, 3060 (1975).
- <sup>22</sup>O. K. Andersen, Z. Pawlowska, and O. Jepsen, *Phys. Rev. B* **34**, 5253 (1986).
- <sup>23</sup>O. K. Andersen and O. Jepsen, *Phys. Rev. Lett.* **53**, 2571 (1984).
- <sup>24</sup>O. K. Andersen, T. Saha-Dasgupta, R. W. Tank, C. Arcangeli, O. Jepsen, and G. Krier, in *Electronic Structure and Physical Properties of Solids: The Use of the LMTO Method*, Lecture Notes in Physics Vol. 535, edited by H. Dreyssé (Springer-Verlag, Berlin, 2000), pp. 3–84.
- <sup>25</sup>H. J. Monkhorst and J. D. Pack, *Phys. Rev. B* **13**, 5188 (1976).
- <sup>26</sup>M. Rohlfling and S. G. Louie, *Phys. Rev. B* **62**, 4927 (2000).
- <sup>27</sup>S. Albrecht, L. Reining, R. Del Sole, and G. Onida, *Phys. Rev. Lett.* **80**, 4510 (1998).
- <sup>28</sup>L. X. Benedict, E. L. Shirley, and R. B. Bohn, *Phys. Rev. B* **57**, R9385 (1998).
- <sup>29</sup>L. X. Benedict and E. L. Shirley, *Phys. Rev. B* **59**, 5441 (1999).
- <sup>30</sup>W. G. Schmidt, S. Glutsch, P. H. Hahn, and F. Bechstedt, *Phys. Rev. B* **67**, 085307 (2003).
- <sup>31</sup>F. Fuchs, C. Rodl, A. Schleife, and F. Bechstedt, *Phys. Rev. B* **78**, 085103 (2008).
- <sup>32</sup>W. R. L. Lambrecht and S. N. Rashkeev, *Phys. Status Solidi B* **217**, 599 (2000).
- <sup>33</sup>W. R. L. Lambrecht and Margarita Prikhodko, *Solid State Commun.* **121**, 549 (2002).
- <sup>34</sup>L. P. Bouckaert, R. Smoluchowski, and E. Wigner, *Phys. Rev.* **50**, 58 (1936).